

This work was written as part of one of the author's official duties as an Employee of the United States Government and is therefore a work of the United States Government. In accordance with 17 U.S.C. 105, no copyright protection is available for such works under U.S. Law.

Public Domain Mark 1.0

<https://creativecommons.org/publicdomain/mark/1.0/>

Access to this work was provided by the University of Maryland, Baltimore County (UMBC) ScholarWorks@UMBC digital repository on the Maryland Shared Open Access (MD-SOAR) platform.

Please provide feedback

Please support the ScholarWorks@UMBC repository by emailing scholarworks-group@umbc.edu and telling us what having access to this work means to you and why it's important to you. Thank you.

Hydroporphyrin-Doped Near-Infrared-Emitting Polymer Dots for Cellular Fluorescence Imaging

Connor Riahin, Adam Meares, Nopondo N. Esemoto, Marcin Ptaszek, Michael LaScola, Narendra Pandala, Erin Lavik, Mengran Yang, Gary Stacey, Dehong Hu, Jeremiah C. Traeger, Galya Orr, and Zeev Rosenzweig*



Cite This: *ACS Appl. Mater. Interfaces* 2022, 14, 20790–20801



Read Online

ACCESS |



Metrics & More



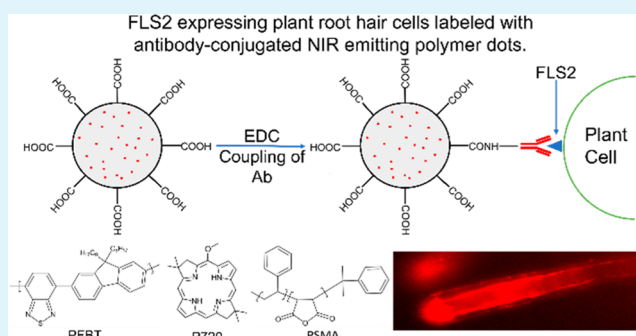
Article Recommendations



Supporting Information

ABSTRACT: Near-infrared (NIR) fluorescent semiconductor polymer dots (Pdots) have shown great potential for fluorescence imaging due to their exceptional chemical and photophysical properties. This paper describes the synthesis of NIR-emitting Pdots with great control and tunability of emission peak wavelength. The Pdots were prepared by doping poly[(9,9-dioctylfluorenyl-2,7-diyl)-alt-co-(1,4-benzo-(2,1',3)-thiadiazole)] (PFBT), a semiconducting polymer commonly used as a host polymer in luminescent Pdots, with a series of chlorins and bacteriochlorins with varying functional groups. Chlorins and bacteriochlorins are ideal dopants due to their high hydrophobicity, which precludes their use as molecular probes in aqueous biological media but on the other hand prevents their leakage when doped into Pdots. Additionally, chlorins and bacteriochlorins have narrow deep red to NIR-emission bands and the wide array of synthetic modifications available for modifying their molecular structure enables tuning their emission predictably and systematically. Transmission electron microscopy (TEM) and dynamic light scattering (DLS) measurements show the chlorin- and bacteriochlorin-doped Pdots to be nearly spherical with an average diameter of 46 ± 12 nm. Efficient energy transfer between PFBT and the doped chlorins or bacteriochlorins decreases the PFBT donor emission to near baseline level and increases the emission of the doped dyes that serve as acceptors. The chlorin- and bacteriochlorin-doped Pdots show narrow emission bands ranging from 640 to 820 nm depending on the doped dye. The paper demonstrates the utility of the systematic chlorin and bacteriochlorin synthesis approach by preparing Pdots of varying emission peak wavelength, utilizing them to visualize multiple targets using wide-field fluorescence microscopy, binding them to secondary antibodies, and determining the binding of secondary antibody-conjugated Pdots to primary antibody-labeled receptors in plant cells. Additionally, the chlorin- and bacteriochlorin-doped Pdots show a blinking behavior that could enable their use in super-resolution imaging methods like STORM.

KEYWORDS: polymer dots, near-infrared, fluorescence microscopy, plant cells, photoblinking, dye-doping, hydroporphyrins



INTRODUCTION

Near-Infrared-Emitting Chlorins and Bacteriochlorins. Fluorescence bioimaging methods, which often rely on the availability of fluorescent probes, are noninvasive, do not require harmful radiation, and offer high spatial resolution and temporal resolution when used to visualize cells, tissues, and even whole animals.¹ Near-infrared (NIR) fluorescent probes are particularly desirable due to lower levels of light scattering with increasing excitation wavelength, reduced tissue autofluorescence in the NIR region of the electromagnetic spectrum, and increased penetration depth and a signal-to-noise ratio, which enable quantitative fluorescence bioimaging of cells and tissues.

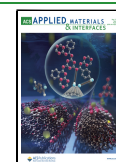
Several classes of NIR dyes have been examined for *in vivo* imaging.^{2,3} Recent examples of small organic molecules used as NIR fluorophores include cyanines⁴ and related dyes,⁵

BODIPY⁶ and aza-BODIPY,⁷ squaraines,⁸ porphyrin derivatives,⁹ and benzobis [1,2,5] thiadiazole.¹⁰ Organic dyes have certain advantages, but they suffer from significant drawbacks, which include poor water solubility, low emission quantum yield when modified to render them water soluble, low photostability, and limited tunability of optical properties. In addition, the optical properties of currently available fluorophores limit their applications for *in vivo* multicolor

Received: March 2, 2022

Accepted: April 8, 2022

Published: April 22, 2022



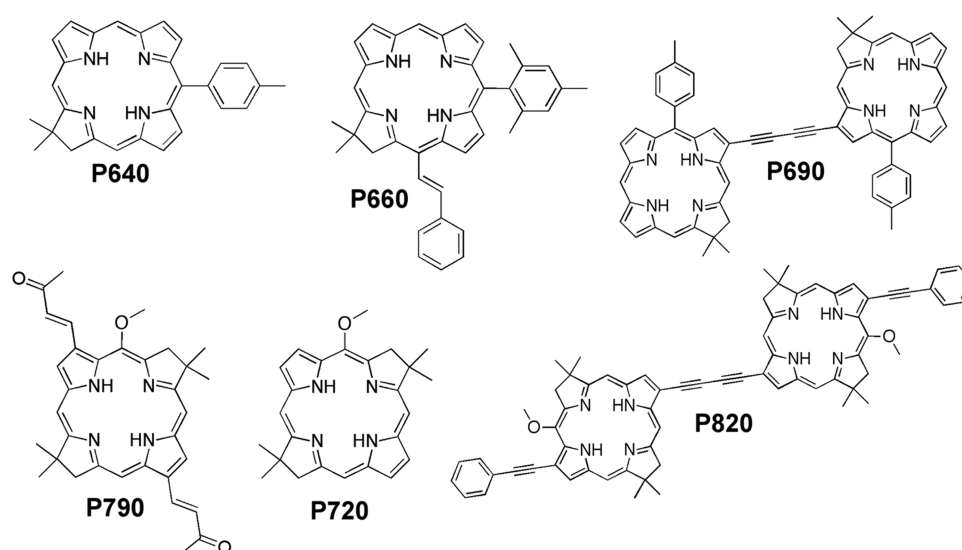


Figure 1. Chemical structures of porphyrins (chlorins and bacteriochlorins) used to prepare the dye-doped Pdts. The notation PXXX stands for porphyrin and its peak emission wavelength.

imaging,² since many NIR agents feature broad emission bands and relatively narrow absorption bands. There is a growing need for new bright, photostable, tunable NIR fluorophores, with optical properties suitable for bioimaging applications in biological aqueous media.

Among different classes of organic fluorophores, hydro-porphyrins (chlorins and bacteriochlorins, Figure 1) appear to have particularly attractive optical properties for multiplexed cellular imaging applications. Chlorins^{11,12} and bacteriochlorins¹³ are synthetic analogues of the photosynthetic pigments chlorophylls and bacteriochlorophylls. These tetrapyrrolic macrocycles differ from well-known porphyrins by having one (chlorins) or two (bacteriochlorins) partially saturated pyrrole rings. They are characterized by relatively strong absorption in the deep red (630–690 nm, $\epsilon \sim 40\,000$ – $80\,000\text{ M}^{-1}\cdot\text{cm}^{-1}$ for chlorins) or NIR (700–800 nm, $\epsilon \sim 100\,000$ – $120\,000\text{ M}^{-1}\cdot\text{cm}^{-1}$ for bacteriochlorins). The emission spectra of both are relatively narrow (FWHM ~ 12 – 25 nm) with quantum yield $\Phi_f \sim 0.20$ – 0.40 (chlorins) and 0.10 – 0.25 (bacteriochlorins). The absorption and emission wavelengths can be tuned across a broad spectral range by either (a) substitution at 3,13-pyrrolic positions of the macrocyclic ring with conjugated, electron-withdrawing, or electron-donating substituents,^{13–15} (b) installation of an additional ring on the periphery of the macromolecule (exocyclic ring),¹⁶ or (c) assembling of the chlorins and bacteriochlorins into strongly conjugated arrays, i.e., arrays where two macrocycles are connected by a linker that provides strong π -conjugation between subunits.¹⁷

NIR Fluorescent Nanoparticles as an Alternative to NIR Molecular Fluorophores. NIR fluorescent dyes generally suffer from poor water solubility,¹¹ and structural modifications to improve their water solubility significantly decrease their emission quantum yield.¹⁸ NIR-emitting nanoparticles, for example, luminescent semiconductor quantum dots (QDs), were developed as an alternative to NIR-emitting molecular probes to overcome their limitations. Luminescent QDs offer several advantages over organic dyes including higher molar absorptivity, broad absorption, large Stokes shifts, and greater photostability.¹⁹ Additionally, luminescent QDs are capable of fluorescing deeper in the IR, with reported

emissions up to 2000 nm.²⁰ A major limitation of QDs, however, is their inherent toxicity, primarily due to (1) leaching of toxic metal ions from the QD core and (2) adverse interactions with the ligands used to stabilize and impart aqueous solubility to the QDs.^{21–24} This is especially true for NIR-emitting QDs, as most are synthesized using Hg- and Pb-based semiconductor nanomaterials.^{25,26} While there have been advances in the development of Hg- and Pb-free NIR-emitting QDs,^{27,28} these newer inorganic nanomaterials still exhibit toxicity due to the leaching of heavy metal ions that continue to limit their *in vivo* applications.²⁹ As such, attention within the field has recently shifted to the development of new nontoxic fluorescent nanoparticles.

Semiconducting polymer nanoparticles, named polymer dots (Pdts), have generated increased interest as a new type of fluorophore, which could provide a viable alternative and overcome some of the major drawbacks of molecular fluorophores and luminescent QDs in the visible and NIR regions.³⁰ Pdts are composed of semiconducting polymers that offer several advantages over inorganic QDs and organic dyes, including facile synthesis, high photostability, tunable absorption and emission, and exceptionally high absorptivity and brightness.³¹ On a per-particle basis, fluorescent Pdts are several times brighter than similar emitting QDs and organic dyes.³⁰ This brightness is the result of fast emissive rates, large extinction coefficients, and high emission quantum yields.³² Additionally, Pdts are resistant to photobleaching,³³ making them highly applicable to fluorescence imaging. Pdts can be synthesized by adding highly emitting hydrophobic polymer molecules dissolved in an organic solvent like tetrahydrofuran (THF) to aqueous solution under vigorous sonication.³⁴ Initial studies using this approach resulted in Pdts characterized by broad emission and low emission quantum yield.³⁵ Modifications of the polymer molecular structure such as the inclusion of π -bridges³⁶ and donor–donor–acceptor systems³⁷ have recently improved the emission quantum yield of Pdts made using this approach. Another approach, which is also used in our study, involves either doping or covalently attaching a NIR-emitting dye to the Pdts.^{38–42} Doping alters the emission properties of the Pdts due to energy transfer between the polymer and the doped dye molecules. The

polymer molecules absorb the excitation light and transfer the energy to the dye molecules. This approach takes full advantage of the properties of both materials: the strong, broad absorption of the polymer and the narrow NIR emission of the dye. Pdots synthesized with this method are significantly brighter on a per-particle basis than the dye alone or similar emitting QDs. A key limitation of NIR-emitting Pdots is the limited availability of NIR dyes and, consequently, the truncated range of possible emission peak wavelengths of NIR-emitting Pdots. Our study successfully increases the selection of NIR-emitting dyes that could be used as efficient acceptors in Pdots, which is necessary to realize the multiplexing potential of NIR-emitting Pdots. This paper describes the synthesis of a series of chlorin- and bacteriochlorin-doped Pdots, which can all be excited by a single excitation source. Systematic modifications of the porphyrin ring result in emission wavelength tenability between 640 and 820 nm. We demonstrated the utility of these red and NIR-emitting Pdots as bioimaging probes in cellular imaging applications and their potential as super-resolution imaging NIR probes.

EXPERIMENTAL SECTION

Chemical Reagents. Poly[(9,9-dioctylfluorenyl-2,7-diyl)-alt-co-(1,4-benzo-(2,1',3)-thiadiazole)] (PFBT) (37 000 MW, 3.3 polydispersity), poly[2-methoxy-5-(3,7-dimethyl-octyloxy)-1,4-phenylene-vinylene] (ADS104) (100 000 MW, 3.3 polydispersity), poly[{9,9-dihexyl-2,7-bis(1-cyanovinylene)fluorenylene}-alt-co-{2,5-bis(N,N'-diphenylamino)-1,4-phenylene}] (ADS111) (48 000 MW, 2.9 polydispersity), and poly[{2-methoxy-5-(2-ethylhexyloxy)-1,4-(1-cyanovinyl)phenylene}-alt-co-{2,5-bis(N,N'-diphenylamino)-1,4-phenylene}] (ADS113) (40 000 MW, 3.5 polydispersity) were purchased from American Dye Source. Poly(styrene/maleic anhydride) (PSMA) [67:33] (MW 7500) was purchased from Polysciences. Tetrahydrofuran (anhydrous, >99.8%), phosphate-buffered saline (PBS), and bovine serum albumin (BSA) were purchased from Fisher Scientific. Dulbecco's modified Eagle medium, fetal bovine serum, HEPES buffer, and sodium pyruvate were purchased from ThermoFisher Scientific. Rat endothelial cells (RECs) were previously isolated in the lab.⁴³ An Anti-Rabbit IgG (H + L), F(ab) fragment antibody produced in goat, N-(3-dimethylaminopropyl)-N'-ethylcarbodiimide, Tris-HCl, NaCl, Driselase, MES, Sodium Azide, Tween 20, and Triton X-100 were purchased from Millipore Sigma. The GST-tag antibody [HRP] produced in rabbits was purchased from GenScript. The nitrocellulose membrane and the Western blot chemiluminescent substrate kit were purchased from Fisher Scientific. Paraformaldehyde (PFA) was purchased from Electron Microscope Sciences. The Murisage and Skoog mixture was purchased from Caisson. The DYKDDDDK Tag Recombinant Rabbit monoclonal antibody was purchased from Invitrogen. All commercial materials were used as received.

Synthesis and Characterization of NIR Porphyrin Dyes. The synthesis and characterization of red-emitting chlorins was previously described.^{44–47} Specifically, the synthesis protocols for P660,⁴⁴ P640,⁴⁶ and P690⁹ as well as near-IR-emitting bacteriochlorins P710^{13,47} and P820¹⁷ were reported previously. The synthesis of P790 is described in detail in the [Supporting Information](#). The notation PXXX stands for porphyrin (P) (chlorin and bacteriochlorins are porphyrins) and the dye's emission peak wavelength. Microwave reactions were performed in a CEM Discover (CEM, Mathew, NC) microwave instrument. All reactions were performed in a 10 mL CEM pressurized microwave vessel, with continuous monitoring of pressure and temperature. The temperature was monitored using a built-in IR sensor. All NMR spectra were acquired on a 400 MHz JOEL ECX-400 NMR.

Polymer Dots (Pdots): Synthesis and Characterization. Porphyrin-doped Pdots were synthesized via a nanoprecipitation

method.³⁸ PFBT, PSMA, and the porphyrin dyes were dissolved in anhydrous THF overnight, each in separate 25 mL round-bottom flasks. Solutions were stored under a nitrogen atmosphere at room temperature, with the dyes stored away from light. The three precursors were filtered through a 0.22 μ m PTFE syringe filter and then mixed together in 1 mL of THF. The concentrations of each of the precursors in the mixture were 100 ppm (PFBT), 100 ppm (PSMA), and 2–20 ppm (dye) depending on the dye. The solution was then injected into 10 mL of DI water under vigorous sonication at room temperature for 1 min. THF was removed through vacuum evaporation on a rotary evaporator at 60°C. All samples were filtered through a 0.22 μ m cellulose acetate syringe filter prior to further studies.

The size and morphology of the synthesized Pdots were measured using an FEI Morgagni 268 100 kV TEM. Samples were prepared by placing a drop of Pdot solution on a Ted Pella copper-supported grid and drying at room temperature. Hydrodynamic size and surface ζ -potential were measured with a DTS1070 folded capillary cell in a Malvern Zetasizer Nano (Model No. ZEN3600) instrument. UV–vis absorption spectra of the Pdots in aqueous solution were measured with an Aligent Cary UV–Vis multicellular Peltier spectrophotometer (Model No. G9864A). Fluorescence spectra of the dye-doped Pdots were measured using a Photon Technology International fluorimeter. All samples were measured in DI water and excited at 450 nm. Corrected spectra were collected from 475 to 850 nm. Fluorescence quantum yields were measured in air-equilibrated solvents using tetraphenylporphyrin (TPP) in air-equilibrated toluene ($\Phi_f = 0.070$)^{DH} as a standard. Fluorescence microscopy experiments were performed using an Olympus ix73 fluorescence microscope equipped with multiple ports. Fluorescence and bright-field images were captured with a Hamamatsu ORCA-Flash4.0 digital CMOS camera. Samples were illuminated by a CoolLED pE-300^{ultra} microscope illuminator. The typical exposure time was 300 ms. For fluorescence spectroscopy images, a Semrock QDLP-B-000 filter cube containing an FF01-435/40-25 excitation filter, an FF01-500/LP-25 emission filter, and an FF510-Di02-25 \times 36 dichroic filter was utilized. Sample spectra of selected areas were captured using an Andor Shamrock SR303i spectrograph equipped with a 150L/MM-500NM grating. The spectra were acquired using a Zyla 4.2 sCMOS camera.

Conjugation of Secondary Antibodies to Pdots. IgG secondary antibody conjugation was achieved through a previously reported method.⁴⁸ A 1 mL aliquot of 100 μ g/mL Pdot solution was mixed with 20 μ L of 5 wt % PEG solution (3350 MW) and 20 μ L of 1 M HEPES buffer. To this mixture, we added 10 μ L of 2 mg/mL IgG secondary antibody solution and stirred the mixture in a vortex to ensure complete mixing. Finally, 20 μ L of 5 mg/mL N-(3-dimethylaminopropyl)-N'-ethylcarbodiimide was added and the mixture was placed on a rotary shaker for 2 h. Afterward, the mixture was transferred to a 100 kDa centrifugal filter unit alongside 10 μ L of 10 wt % Triton X-100 and centrifuged at 5000 RCF for 10 min to remove the unbound antibody. Conjugation was confirmed using dynamic light scattering and ζ -potential measurements and Dot Blot. In Dot Blot experiments, a Goat Anti-Rabbit IgG secondary antibody (original 2 mg/mL, used as the positive control), pure Pdots (used as negative control), and antibody-conjugated Pdots were diluted by 10-fold multiple times, and 2 μ L of each sample was spotted onto the nitrocellulose membrane. After blocking nonspecific sites by soaking in 5% skim milk powder dissolved in TBST buffer (20 mM Tris-HCl pH 7.5, 150 mM NaCl, 0.1 % Tween 20) for 0.5–1 h, the nitrocellulose membrane was incubated with the primary antibody conjugated with HRP (GST-tag antibody [HRP] produced in rabbit) for 1 h at RT. Afterward, the nitrocellulose membrane was washed three times with TBST buffer (3 \times 5 min) and incubated with the Western blot chemiluminescent substrate for 1 min and then was used to expose X-ray films in the dark room.

Cellular Imaging and Toxicity Studies. Rat endothelial cells cultured in Dulbecco's modified Eagle medium (DMEM) high glucose supplemented with 10% FBS, 1% HEPES, and 1% sodium pyruvate were used in our cellular imaging studies. Cell viability measurements were carried out by seeding \sim 50 000 cells in each well

of a 24-well plate and allowing the cells to grow for 24 h. The cells were then washed twice with phenol red- and serum-free DMEM. Pdots (~10 and 50 $\mu\text{g/mL}$) were then added to the cells after being filtered and diluted in phenol red-free and serum-free DMEM and incubated for 1 h. Calcein-AM and ethidium homodimer were then added to the cells at concentrations of 4 and 2 μM , respectively. For the negative control, cells were incubated with 70% ethanol to ensure complete cell death. The medium was removed from the well before imaging so the excess Pdots in solution do not interfere with the fluorescing cells, but the wells were not washed so as not to remove any dead cells. The cells were then imaged and processed using a Cytation 5 fluorescence microscope with Gen5 imaging software (Biotek). Cell quantification was performed using ImageJ, counting with the multipoint tool. Cellular imaging and spectroscopy measurements with Pdots were carried out by seeding about 100 000 cells in each well and allowing the cells to grow for 24 h. The cells were then washed twice with phenol red- and serum-free DMEM. Single-type or mixed Pdots were added to the wells and incubated with the cells for 30 min at 37 $^{\circ}\text{C}$. The cells were then washed twice with phenol red- and serum-free DMEM to remove excess Pdots not taken up by the cells. Cells were then imaged using an Olympus ix73 fluorescence microscopy system described above.

Construction of FLAG–FLS2 Transgenic Plants. The FLAG sequence-fused FLS2 genomic fragment was generated by a two-fragment polymerase chain reaction (PCR) approach, in which primers including the FLAG sequence were used in two separate PCR reactions. Each fragment of FLS2 was amplified by PCR from the genomic DNA of wild-type plants using gene-specific primers containing the FLAG sequence. An overlapping PCR reaction was then performed to generate the whole FLS2 genomic fragment with the FLAG sequence inserted behind the signal peptide sequence of FLS2. The PCR products were cloned into pDONR-Zeo (Invitrogen) by BP reaction and subsequently cloned into the binary vector pGWB1 (Invitrogen) by LR reaction. The construct was then transformed into *Arabidopsis thaliana* fls2 knockout mutant plants via the Agrobacterium strain GV3101 using the “floral-dip” method.⁴⁹ The fls2 knockout mutant was obtained from the Arabidopsis Biological Resource Center (ABRC, Ohio State University, Columbus, OH). The transgenic plants were selected by germination on a 35 $\mu\text{g/mL}$ hygromycin-containing 1/2 MS medium. Homozygous T3 generation plants were used in this study. The functionality of the FLAG-tagged FLS2 receptor was confirmed by its ability to complement the phenotype of the fls2 knockout mutant.

Fluorescence Imaging of Antibody-Conjugated Pdots When Targeting the FLS2 Receptor in Plant Cells. *A. thaliana* seeds, expressing FLAG-tagged FLS2 (FLAG–FLS2) at the N terminus, were grown on 0.5% phytagel with Murisage and Skoog media for 10–14 days with photocycles of 16 h of light followed by 8 h of darkness. Plants were removed from the medium and fixed in 4% Paraformaldehyde for 1 h under vacuum before being stored in PBS. Prior to immunostaining, a scalpel was used to slice the leaves to allow some chlorophyll release for clearer imaging. The plant cell wall was partially dissolved by 0.2% driselase in 2 mM MES at pH = 5.7 at 37 $^{\circ}\text{C}$ for 15 min. The membrane was then permeabilized with 1% Triton X-100 in PBS for 20 min at room temperature. Plants were then soaked in blocking buffer (1% BSA, 0.1% tween, 2 mM sodium azide in PBS) at room temperature for 20 min. Primary Rabbit anti-DYKDDDDK-tag (anti-FLAG) antibodies were diluted to 1:250 in blocking buffer, and plants were incubated with primary antibodies overnight at 4 $^{\circ}\text{C}$. Plants were rinsed in blocking buffer three times for 20 min at room temperatures. Pdots conjugated to the secondary antibody (Goat Anti-Rabbit IgG) were then diluted to 30 $\mu\text{g/mL}$ in blocking buffer and incubated for 3 h at room temperature. Plants were rinsed in PBS three times for 10 min at room temperature.

Leaves and root hairs were removed from the plant and placed in a glass-bottom dish with 10 μL of PBS under a 10 cm glass coverslip. These were imaged using an inverted fluorescence microscope (Olympus IX73). These were illuminated using a 440 nm solid-state laser (Crystalaser) at 0.1 mW. Samples were observed using a 60 \times magnification, water objective lens (NA 1.2, Olympus

UPlanSApo). Images were collected through a 647 nm band pass filter with 57 nm width and a 710 nm band pass filter with 40 nm width. Images were captured by an EMCCD camera (Princeton Instrument Photonmax) at 0.3 s exposure time.

Fluorescence Imaging of Single Pdots. Pdots were diluted in water, placed on a glass coverslip, and imaged using the inverted fluorescence microscope and laser described in the previous section. Pdot samples were observed using a 100 \times magnification, oil immersion objective lens (NA 1.4, Olympus UPlanSApo). The laser illumination covered an area with a diameter of ~ 80 μm . Emission was acquired using a band pass filter centered at 647 nm with 57 nm width.

RESULTS AND DISCUSSION

Chlorin and Bacteriochlorin, Molecular Design, Synthesis, and Characterization. Chlorins and bacteriochlorins are uniquely characterized by narrow emission bands compared to other NIR-emitting dyes with the full-width at half-maximum (FWHM) of ~ 15 nm for chlorins and ~ 20 nm for bacteriochlorins.^{11–13,50} In addition, unlike with other NIR-emitting dyes, it is possible to position and tune the emission band of chlorins and bacteriochlorins with nearly nanometer precision.^{11–13,50} Tuning the absorption band of chlorins and bacteriochlorins is realized by changing their molecular structure, specifically by substituting functional groups at the periphery of their macrocycles. Conjugated or electron-withdrawing/electron-donating substituents affect the HOMO–LUMO energies and consequently $S_0 \rightarrow S_1$ transitions energies.^{11–13,50} A second way to tune the emission wavelength of chlorins and bacteriochlorins involves arranging their macrocycles into conjugated arrays. Conjugation of the macrocycles delocalizes molecular orbitals over adjacent macrocycles, thus increasing the size of the π -system. This ultimately leads to a reduction of the $S_0 \rightarrow S_1$ energy bandgap.¹⁵ In the current study, we prepared NIR-emitting Pdots using a series of hydrophobic chlorins and bacteriochlorins we previously synthesized (Figure 1), in which all share a common hydroporphyrin macrocyclic structure. The chlorin and bacteriochlorin dyes differ in their peripheral substituents, or they are arranged into strongly conjugated arrays. The set includes a simple chlorin P640, which possesses the shortest emission wavelength, styrene-substituted P660, and a conjugated dyad 690, for which the emission wavelength is progressively bathochromically shifted. Similarly, we also used a bacteriochlorin series that contains a simple bacteriochlorin P720, chalcone-substituted P790, and a conjugated dyad P820. Chalcone substituent,⁵¹ which is both conjugated and electron withdrawing, significantly shifts the absorption of P790 compared to P720. The strongly conjugated dyads P690 and P820 are the most bathochromically shifted derivatives in both the chlorin and the bacteriochlorin series. As described in detail in the **Experimental Section**, substituted chlorins and bacteriochlorins were prepared using palladium-catalyzed cross-coupling reactions, starting from the corresponding monobromochlorins and dibromo-bacteriochlorins, respectively.^{44–46} For example, Scheme S1 shows the synthesis of P790 using a microwave-assisted Heck reaction^{44,51} of a known bacteriochlorin- Br_2 ⁴⁷ and methyl vinyl ketone with a 46% yield. Structures of the six porphyrin dyes used in this study are shown in Figure 1. The full synthetic procedure to prepare P790, its NMR characterization, and UV–vis and fluorescence spectra for all dyes are shown in the Supporting Information (Figures S1–S6).

Polymer Selection for NIR-Emitting Pdots. An appropriate selection of a semiconducting polymer for fluorescent Pdots is imperative for their optical properties. In our NIR-emitting Pdots, the Pdots are excited at the peak absorption maximum of the polymer molecules. The emission maximum is obtained at the emission peak wavelength of the doped NIR dye. High absorption cross section at the excitation wavelength and efficient energy transfer between the polymer and dye molecules are imperative for high NIR emission of the Pdots. Additionally, the emission band of the polymer should minimally bleed into the emission peak of the doped dye to minimize spectral interference between the polymer and dye molecules in imaging experiments. Figure 2 shows the

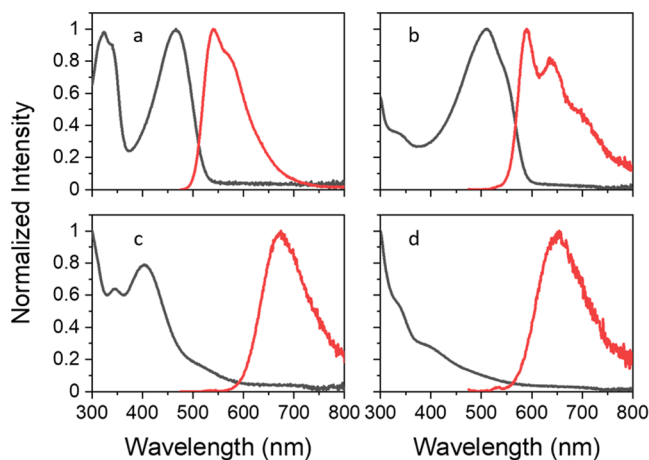
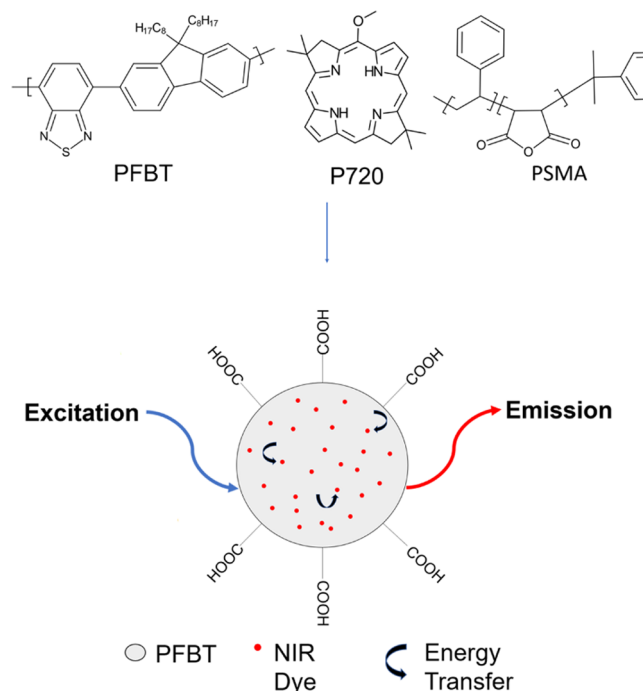


Figure 2. Absorption (black) and fluorescence (red) spectra of (a) PFBT, (b) ADS104, (c) ADS 111, and (d) ADS113.

normalized UV–vis and fluorescence spectra of four semiconductor fluorescent polymers PFBT (Figure 2a), ADS104 (Figure 2b), ADS 111 (Figure 2c), and ADS114 (Figure 2d). The three polymers from the ADS series have been used previously in Pdots⁴⁷ but they show lower emissions than PFBT and more importantly, their emission peak tails bleed into the NIR region. PFBT was chosen as the polymer for our NIR-emitting Pdots because of its high absorption cross section and sufficient overlap of its fluorescence peak with the absorption peaks of our porphyrin dyes, conveniently excitable absorbance peak, and most importantly, its minimal overlap of the emission peak red tail with the dyes' emission. Using PFBT as the polymer component of the Pdots has enabled the formation of Pdots with emission peak wavelengths ranging from 640 to 820 nm. It is possible to further tune Pdots' emission by using blue shifted-emitting polymers for visible-emitting Pdots or by using red shifted-emitting polymers like ADS104, ADS 111, and ADS113 for Pdots that emit even deeper into the NIR region.

Synthesis and Characterization of NIR-Emitting Pdots. Chlorin and bacteriochlorin dyes used in our study are hydrophobic and cannot be used as molecular probes in aqueous media without incorporating them into Pdots. The synthesis of chlorin- and bacteriochlorin-doped Pdots is shown in Scheme 1. As described in the Experimental Section, the NIR-emitting Pdots are prepared by injecting PFBT, PSMA, and fluorescent dye mixture, all dissolved in THF, into aqueous solution under vigorous sonication following a previously described Pdots' synthesis protocol.³⁸ Large

Scheme 1. Preparation of Dye-Doped NIR-Emitting Polymer Dots (Pdots) (Shown Here With P720)



aggregates that form during the short 1-min-long reaction are removed from the Pdots' solution by filtration.

The structural properties of the formed Pdots are shown in Figure 3. A representative TEM image (Figure 3a) and size distribution (Figure 3b) of the formed Pdots show near-spherical morphology with some disorder in structure and an average diameter of 46 ± 12 nm. While the obtained Pdots are fairly polydisperse, their emission peak wavelength is independent of their size. As expected, DLS measurements show a slightly larger average hydrodynamic diameter of 52 nm (Figure 3c). The surface ζ -potential, shown in Figure S7 of the synthesized Pdots, was -37 mV; indicating that the surface is functionalized with negatively charged carboxyl groups.

Pdots' NIR-Emission Properties. Due to the spectral overlap between the PFBT emission and porphyrin absorption, and the close proximity of the dyes to the polymer when doped into a Pdot, we predicted a highly efficient energy transfer from the polymer to the dye upon excitation of the porphyrin-doped PFBT Pdots at 450 nm. As expected, doping PFBT Pdots with optimal dye concentration resulted in complete quenching of PFBT fluorescence and in an increase in NIR emission from the dopant dyes. Figure 4 shows normalized fluorescence spectra of all six NIR-emitting Pdots. The formed porphyrin-doped Pdots feature narrow emission peaks in the NIR range with an average full-width at half-maximum (FWHM) of 25 nm. Table 1 summarizes the emission peak wavelength and emission quantum yield of the porphyrin dyes (termed PXXX) and porphyrin-doped Pdots (termed PPDXXX). An emission red shift is observed when the dyes are doped into the Pdots most likely due to changes in their chemical environment. The magnitude of the red shift is larger at higher emission peak wavelengths. Consistent with previous studies,³⁸ the emission quantum yields of the dye-doped Pdots are lower than the emission quantum yield of dye-free PFBT Pdots but the emission peaks are significantly narrower and in the NIR region. The emission quantum yields of the formed NIR-

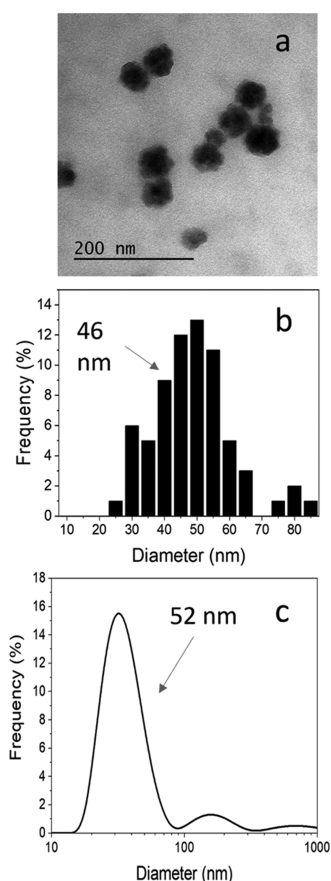


Figure 3. (a) Size and morphological characterization of PFBT polymer dots (loaded with P640) by TEM. The representative TEM image shows the near-spherical Pdots to average 46 ± 12 nm in diameter with some disorder. (b) Histogram of Pdots' size distribution from TEM images ($n = 69$) shows the Pdots to be somewhat polydispersed and the formation of larger aggregates. (c) Dynamic light scattering (DLS) measurements show the Pdots' hydrodynamic diameter to an average of 52 nm, which is in close agreement with the TEM results.

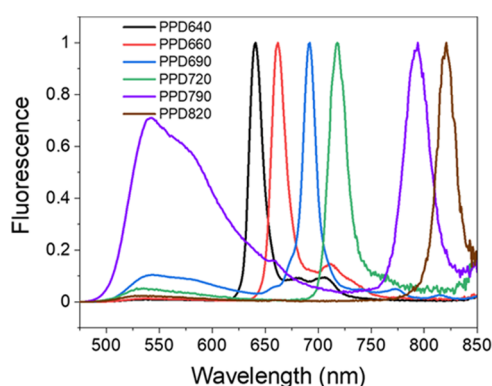


Figure 4. Normalized emission spectra of porphyrin-doped polymer dots ($\lambda_{\text{ex}} = 450$ nm).

emitting Pdots range from 0.1 to 0.5 with no apparent trend. The amount of the dye dopant in the Pdots was optimized by varying the dopant concentration in the Pdots' preparation solution to maximize their fluorescence intensity. The NIR-emission intensity of the Pdots increases with increased dye concentration up to a certain optimum level. Within this concentration range, the polymer emission is drastically

Table 1. Peak Emission Wavelengths and Fluorescence Quantum Yields of Porphyrin Dyes in THF and PPDs in Water

sample	λ_{em} dye (nm)	λ_{em} PPD (nm)	QY dye	QY PPD
P640	637	641	0.29 ± 0.01	0.11 ± 0.01
P660	657	662	0.52 ± 0.02	0.49 ± 0.01
P690	686	692	0.35 ± 0.01	0.21 ± 0.01
P720	711	718	0.31 ± 0.01	0.20 ± 0.01
P790	778	794	0.25 ± 0.01	0.20 ± 0.01
P820	800	821	0.32 ± 0.01	0.15 ± 0.01

reduced, and the dye emission increases. Above a certain doping percentage, the dye emission begins to decrease due to self-quenching. For example, for PPD640, a P640 concentration in the reaction mixture of 6.9% resulted in the highest emission, and the NIR emission decreased above this level (data not shown). The PFBT native emission also increases when the excitation intensity is above the saturation level of the dye-doped Pdots. An example of the saturation effect is shown in Figure 3 for PPD790 (purple curve). While energy transfer between PFBT and P790 molecules results in NIR emission at 790 nm, the emission of PFBT is only partially quenched even at a P790 level of 9.1%, the level required to maximize the PPD790 NIR emission. This may be attributed to molecular interactions that inhibit energy transfer from the polymer to the dye molecules that need to be further studied. To prevent dye fluorescence quenching and saturation, we set the dye loading percentage to an optimal level of 5% in all of the Pdots used in this study.

Cellular Imaging and Toxicity Studies. A common concern associated with the use of fluorescent nanoparticles, in our study NIR-emitting Pdots, is whether they by themselves affect cell viability during incubation. Cell viability stain assays using Calcein-AM and ethidium homodimer-1 were carried out to determine whether our NIR-emitting Pdots adversely impact cell viability upon exposure and incubation. Calcein-AM, a green fluorescent dye, is readily endocytosed by live cells; while ethidium homodimer, a red fluorescent dye, is only capable of penetrating dead cells. Fluorescence images of cells labeled with our Pdots compared to a positive control are shown in Figure 5. Figure 5a–c shows that cells incubated for 1 h with PPD640 concentrations 0, 10, and 50 $\mu\text{g/mL}$, respectively, had almost no fluorescence from the homodimer; indicating that most of the cells remained viable including at high concentrations of Pdots. Cell viability assays conducted following incubating the cells with NIR emitting Pdots for 24 h further support our finding that the Pdots do not adversely impact the cells when used as cellular imaging probes in cellular imaging studies.

To demonstrate the multiplexing capabilities of our dye-doped Pdots, we incubated rat endothelial cells with a mixture of Pdots of varying emission wavelengths. Endothelial cells have been shown to readily endocytose nanoparticles of similar dimensions to our Pdots.^{52,53} Bright-field and fluorescence microscopy images of cells incubated with PPD640, PPD660, and PPD690 Pdots are shown in Figure 6. Figure 6a,b shows bright-field and fluorescence images of cells labeled with one type of PPDs, PPD640. The bright-field image in Figure 6a shows that the PPD-labeled cells maintain their structural integrity. The fluorescence image in Figure 6b shows some of the PPDs attached to the cells' membranes, while others may have permeated into the cells. The inset in Figure 6b shows the

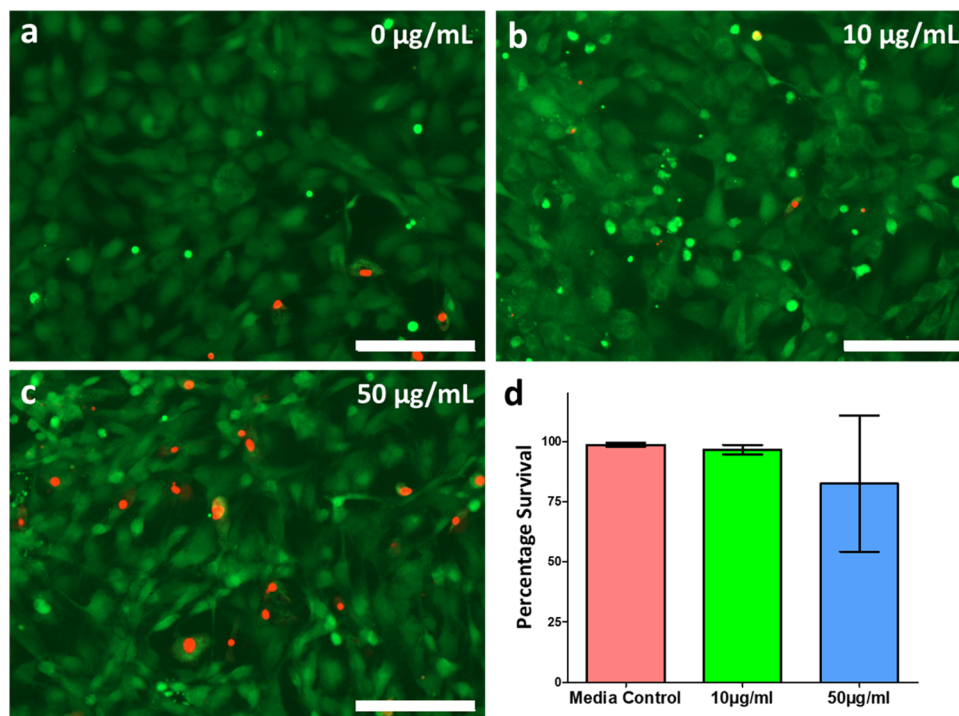


Figure 5. Live/dead RECs incubated for 1 h at 37 °C in the presence of P640-loaded Pdts at (a) 0 µg/mL, (b) 10 µg/mL, and (c) 50 µg/mL (scale bar: 200 µm). Calcein-AM (green) stain is used to stain live cells and ethidium homodimer-1 (red) is used to stain dead cells. (d) Survival percentage of RECs with Pdts at different concentrations.

fluorescence spectra of the subsection of the fluorescence image with high Pdot density. As expected, it shows a single fluorescence peak at 640 nm. Figure 6c,d shows bright-field and fluorescence images of cells labeled with two types of NIR-emitting Pdts, PPD640 and PPD660. The inset in Figure 6d shows the presence of the two types of PPDs in the cells. Figure 6e,f shows bright-field and fluorescence images of cells labeled with three types of NIR-emitting Pdts, PPD640, PPD660, and PPD690. The inset of Figure 6f shows the presence of the three types of PPDs in the cells. While a baseline separation of emission peaks is not realized over the narrow emission wavelength range of about 70 nm used in these measurements, our results clearly indicate that due to their narrow emission peaks our NIR-emitting Pdts could be used for multiplex cellular fluorescence imaging of multiple targets either in the cell or on the cell membrane.

Fluorescence Imaging of Targeted Receptors in Plant Cells. NIR spectrum fluorescent dyes are a promising avenue for bioimaging in plants, as the presence of chlorophyll limits the types of fluorescent dyes available within the visible spectrum. The emission spectrum for Chlorophyll-*b* includes a peak from ~600 to 670 nm, thus NIR dyes that emit at longer wavelengths may not be obscured by a strong chlorophyll background, making them ideal candidates for fluorescence imaging in leaves. To demonstrate the potential for the use of NIR Pdts for bioimaging in plants, we first conjugated Anti-Rabbit IgG (H + L), F(ab) fragment antibody molecules to P690 containing Pdts (PPD690). The conjugation of antibody molecules to the Pdts was confirmed by dynamic light scattering (DLS), which showed an increase in the hydrodynamic diameter from 46 ± 12 to 70 ± 10 nm and ζ -potential from -47.8 to -34.5 mV. The activity of the antibody–Pdot conjugates was confirmed using Dot Blots, which showed a clear recognition of the primary antibody

produced in rabbits by the Anti-Rabbit IgG (H + L), F(ab) fragment antibody-conjugated Pdts. We then stained the transmembrane receptor kinase FLAGELLIN SENSITIVE2 (FLS2) in both leaf cells and root hair cells of *A. thaliana*. Both cell types express the FLS2 receptors, which play a key role in recognizing the bacterial flagellin protein and, hence, generating a defense reaction to the invading bacterial pathogen.^{54,55} The *A. thaliana* plants were genetically engineered to express a DYKDDDDK peptide, known as FLAG, tag at the FLS2 receptor N terminal. The functionality of this transgenic receptor construct was confirmed by showing that it restored flagellin recognition to *A. thaliana* fls2 mutant plants.

To demonstrate the utility of our Anti-Rabbit IgG (H + L), F(ab) fragment antibody-conjugated Pdts, plants expressing the FLAG-tagged FLS2 receptor were stained with a DYKDDDDK Tag Recombinant Rabbit Monoclonal Antibody. Plants were then rinsed and stained with Anti-Rabbit IgG (H + L), F(ab) fragment antibody-conjugated PPD690 Pdts. This staining was performed alongside a wild-type control plant lacking the FLAG-tagged FLS2 receptor. We imaged these plants on an inverted fluorescence microscope illuminated by a 440 nm laser in both 647 and 710 nm channels. To decrease chlorophyll interference in the leaf, small cuts were made in the leaves to allow the release of some chlorophyll, which enabled us to resolve fluorescent Pdts along the leaf cell walls in both channels (Figure 7A, left). In contrast, no specific staining was observed in the wild type (Figure 7A, right). The same results occurred when imaging root hair cells, showing specific fluorescence signals in both channels in the FLAG-tagged FLS2 plants but not in the wild-type plants (Figure 7B). These results demonstrate that the antibody-coated PPD690 Pdts were able to specifically bind to FLAG-tagged receptors within fixed plant tissues. While

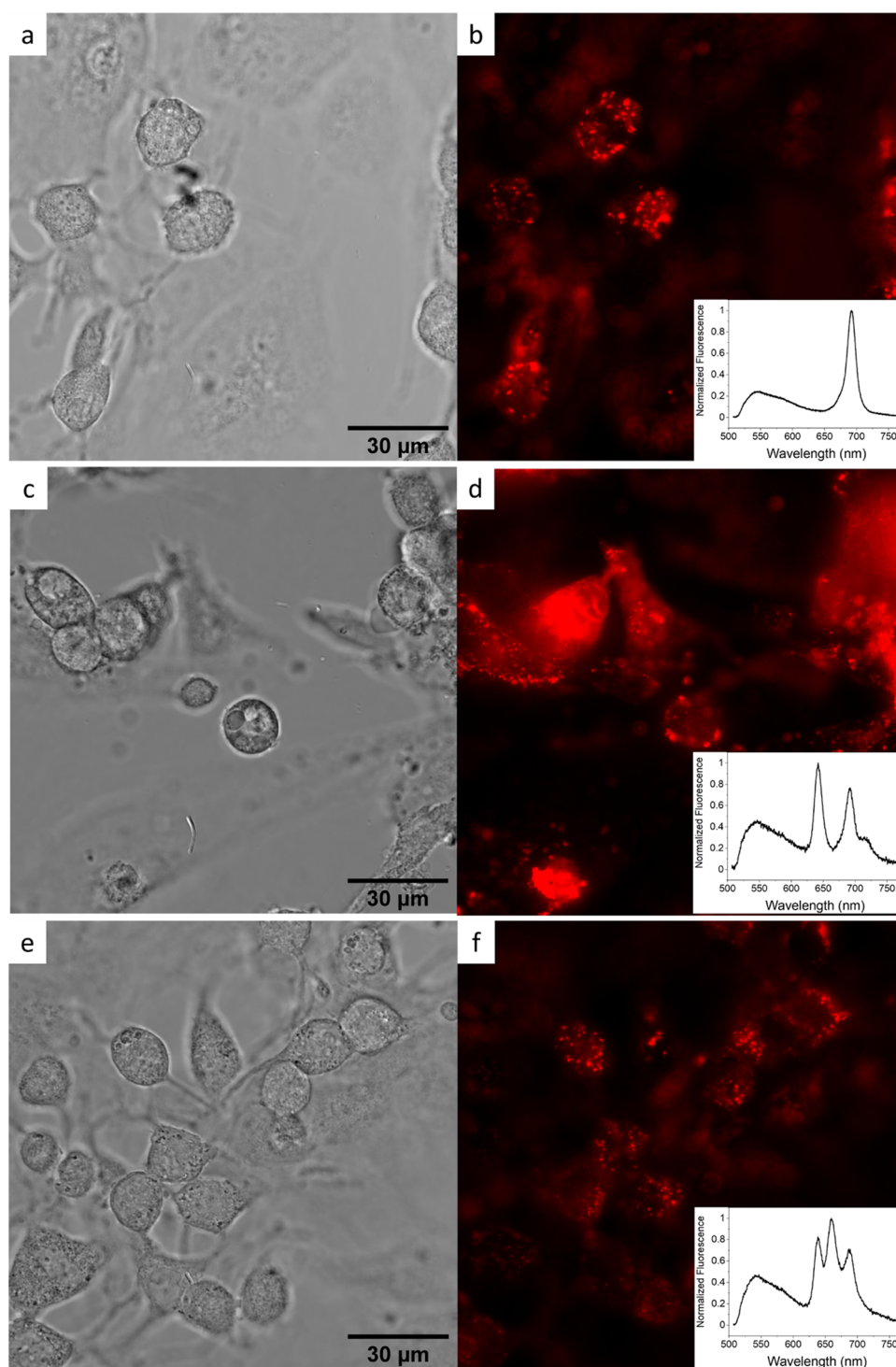


Figure 6. Bright-field and fluorescence images of rat endothelial cells incubated with (a, b) one type of NIR-emitting Pdts PPD640, (c, d) two types of NIR-emitting Pdts PPD640 and PPD660, and (e, f) three types of NIR-emitting Pdts PPD640, PPD660, and PPD690. Insets show the fluorescence spectra of subsections of the image with high Pdot density.

ideally NIR Pdts in longer wavelengths will be used to circumvent the presence of chlorophyll within leaves by emitting at wavelengths beyond the chlorophyll emission spectrum, these results demonstrate as a proof of concept that antibody-conjugated Pdts within our experimental system are able to specifically recognize their target in plant tissues.

Fluorescence Blinking of Pdts. While NIR fluorescence imaging microscopy is advantageous due to the reduced autofluorescence background, its spatial resolution is diffrac-

tion-limited. Therefore, the increase in emission wavelengths decreases the spatial resolution of microscopy experiments compared to fluorescence microscopy measurements in the visible region. To overcome this spatial resolution limitation, we conducted single-particle imaging studies to determine whether our 50 nm NIR-emitting Pdts could be used as super-resolution imaging probes. When an aqueous solution of PPD690 Pdts was diluted and imaged with high magnification, it was possible to capture emissions of individual Pdts as

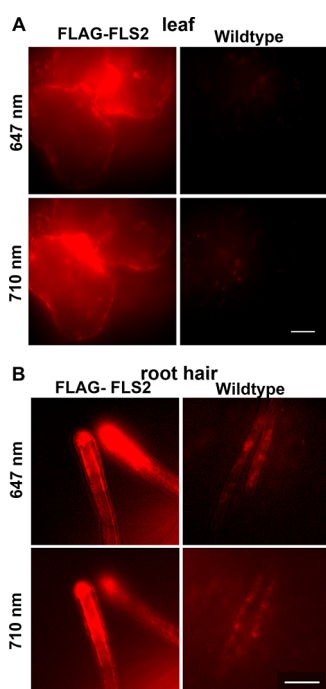


Figure 7. Examples of fluorescence images showing leaf cells (A) and root hair cells (B) taken from *A. thaliana* expressing Flagellin Sensitive2 (FLS2) receptor kinase tagged with FLAG at the N-terminal (left panel) and from a wild-type plant expressing FLS2 with no tag serving as the negative control (right panel). The receptor is labeled using a primary antibody against FLAG, followed by PPD690 (Pdots encapsulating the P690 dye), and decorated with a secondary antibody against the primary antibody. Images were taken in two channels to capture the emissions of the polymer (647 ± 57 nm, upper) and the emission of the dye (710 ± 40 nm, lower). Scale bars represent $20 \mu\text{m}$.

they went through on–off cycles or blinking. This blinking behavior is demonstrated in Figure 8, where consecutive images are selected from a series, available under the Supporting Information (Video 1). Such a blinking property makes these Pdots valuable for single-molecule-based super-

resolution fluorescence imaging, such as STORM⁵⁶ or PALM,⁵⁷ where photoswitching fluorophores are required. Together with the observation that these Pdots are not toxic to living cells, their ability to blink makes them valuable for biological imaging with nm spatial resolution.

SUMMARY AND CONCLUSIONS

This paper describes the synthesis of deep red- and NIR-emitting Pdots that were prepared by doping Pdots with a series of chlorin and bacteriochlorin dyes with systematically tuned molecular structures. The resulting Pdots are excited by a single excitation source and are highly emitting with distinct narrow emission peaks and high emission quantum yields over a broad range of emission wavelengths. Doping the Pdots with chlorins and bacteriochlorins minimally alters the emission properties of the free dyes and enables their use in aqueous biological buffers. It is very challenging to use chlorins and bacteriochlorins in a free form in aqueous media because of their low aqueous solubility. The study reveals that the resulting Pdots do not show measurable cytotoxicity under our experimental conditions of a relatively short Pdot–cell exposure of 1 h. We demonstrated the utility of the porphyrin-doped Pdots in multiplexed cellular imaging. We also show that when labeled with secondary antibodies, the NIR-emitting Pdots can be used effectively for targeted imaging of receptors in plant cells. NIR imaging is especially important in plant cells where autofluorescence of chlorophyll and other cellular constituents in the visible range of the electromagnetic spectrum is often a limiting factor. Finally, the data show that the porphyrin-doped NIR-emitting Pdots photoblink and therefore could potentially be used as super-resolution cellular imaging probes. However, our study also reveals that while chlorin- and bacteriochlorin-doped Pdots are sufficiently photostable and could be used effectively in wide-field fluorescence imaging applications, their limited photostability hinders their use in super-resolution imaging studies. Currently, we are exploring a new series of dyes with greatly improved photostability for preparing Pdots for super-resolution imaging applications.

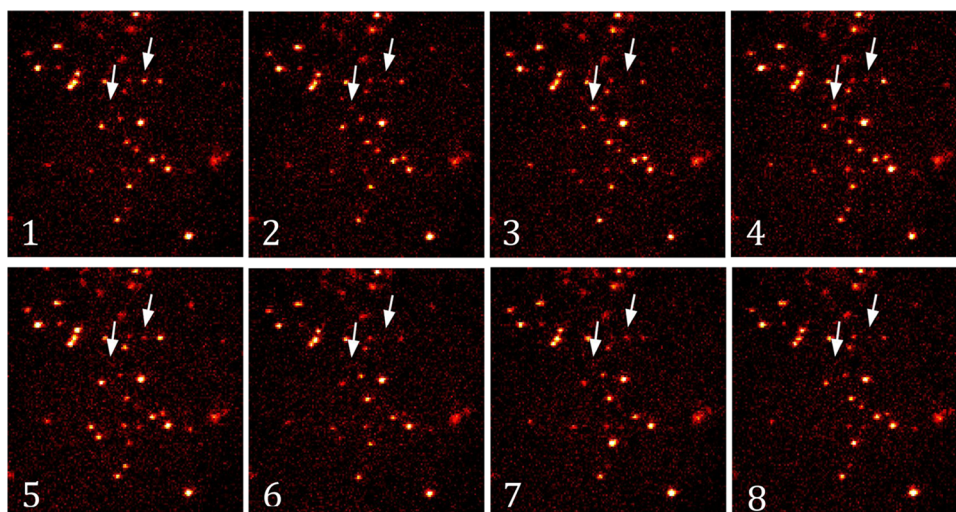


Figure 8. Demonstration of Pdot blinking. Consecutive images of PPD640 Pdots selected from a series shown in the Supporting Video. The Pdots were diluted and imaged on a glass coverslip using a 440 nm excitation wavelength and an ~ 600 to 700 nm emission band. The arrows point to two Pdots as an example of their blinking through the series.

■ ASSOCIATED CONTENT

SI Supporting Information

The Supporting Information is available free of charge at <https://pubs.acs.org/doi/10.1021/acsami.2c02551>.

Detailed information about the synthesis and characterization of bacteriochlorin P790 (Scheme S1 and Section 1.1), the absorption and emission spectra of the chlorin and bacteriochlorin dyes used in the study (Figures S1–S6 in Section 1.2), and ζ -potential of the Pdots (Figure S7 in Section 1.3) (PDF)

Supporting Video (AVI)

■ AUTHOR INFORMATION

Corresponding Author

Zeev Rosenzweig – Department of Chemistry and Biochemistry, University of Maryland, Baltimore County, Baltimore, Maryland 21250, United States; orcid.org/0000-0001-6098-3932; Email: zrosenzw@umbc.edu

Authors

Connor Riahin – Department of Chemistry and Biochemistry, University of Maryland, Baltimore County, Baltimore, Maryland 21250, United States

Adam Meares – Department of Chemistry and Biochemistry, University of Maryland, Baltimore County, Baltimore, Maryland 21250, United States

Nopondo N. Esemoto – Department of Chemistry and Biochemistry, University of Maryland, Baltimore County, Baltimore, Maryland 21250, United States; orcid.org/0000-0001-5212-4484

Marcin Ptaszek – Department of Chemistry and Biochemistry, University of Maryland, Baltimore County, Baltimore, Maryland 21250, United States; orcid.org/0000-0001-6468-6900

Michael LaScola – Department of Chemical, Biological and Environmental Engineering, University of Maryland, Baltimore County, Baltimore, Maryland 21250, United States

Narendra Pandala – Department of Chemical, Biological and Environmental Engineering, University of Maryland, Baltimore County, Baltimore, Maryland 21250, United States

Erin Lavik – Department of Chemical, Biological and Environmental Engineering, University of Maryland, Baltimore County, Baltimore, Maryland 21250, United States; orcid.org/0000-0002-0644-744X

Mengran Yang – Division of Plant Sciences and Biochemistry, University of Missouri, Columbia, Missouri 65211, United States

Gary Stacey – Division of Plant Sciences and Biochemistry, University of Missouri, Columbia, Missouri 65211, United States

Dehong Hu – Environmental Molecular Sciences Laboratory, Pacific Northwest National Laboratory, Richland, Washington 99354, United States; orcid.org/0000-0002-3974-2963

Jeremiah C. Traeger – Environmental Molecular Sciences Laboratory, Pacific Northwest National Laboratory, Richland, Washington 99354, United States

Galya Orr – Environmental Molecular Sciences Laboratory, Pacific Northwest National Laboratory, Richland,

Washington 99354, United States; orcid.org/0000-0002-5552-2151

Complete contact information is available at: <https://pubs.acs.org/doi/10.1021/acsami.2c02551>

Notes

The authors declare no competing financial interest.

■ ACKNOWLEDGMENTS

The study is primarily supported by the US Department of Energy Basic Energy Research (DOE-BER) grant DE-SC0020346. C.R.'s and N.N.E.'s doctoral studies are partially supported by NIH Chemistry–Biology Interface (CBI) training grant NIH/NIGMS T32 GM066706. N.N.E. is also partially supported by the Meyerhoff Graduate Program at UMBC, which is supported by NIH-NIGMS initiative for maximizing student development (Grant No. 2 R25-GM55036). Postdoctoral support for M.Y. was provided by a grant from the National Science Foundation Plant Genome Program (Grant No. IOS-2048410). A portion of this research was performed at the Environmental Molecular Sciences Laboratory, a DOE Office of Science User Facility sponsored by the Biological and Environmental Research program under Contract No. DE-AC05-76RL01830.

■ REFERENCES

- (1) Tsai, W.; Yang-Hsiang, C. Semiconducting Polymer Dots as Near-Infrared Fluorescent Probes for Bioimaging and Sensing. *J. Chin. Chem. Soc.* **2019**, *66*, 9–20.
- (2) Ptaszek, M. Rational Design of Fluorophores for In Vivo Applications. *Prog. Mol. Biol. Transl. Sci.* **2013**, *113*, S9–108.
- (3) Hong, G.; Antaris, A.; Dai, H. Near-Infrared Fluorophores for Biomedical Imaging. *Nat. Biomed. Eng.* **2017**, *1*, No. 0010.
- (4) Nani, R. R.; Gorka, A. P.; Nagaya, T.; Yamamoto, T.; Ivanic, J.; Kobayashi, H.; Schnermann, M. J. In Vivo Activation of Duocarmycin-Antibody Conjugates by Near-Infrared Light. *ACS Cent. Sci.* **2017**, *3*, 329–337.
- (5) Gao, X.; Ma, G.; Jiang, C.; Zeng, L.; Jiang, S.; Huang, P.; Lin, J. In Vivo Near-Infrared Fluorescence and Photoacoustic Dual-Modal Imaging of Endogenous Alkaline Phosphatase. *Anal. Chem.* **2019**, *91*, 7112–7117.
- (6) Inagaki, F. F.; Fujimura, D.; Ansteatt, S.; Okada, R.; Furusawa, A.; Choyke, P. L.; Ptaszek, M.; Kobayashi, H. Effect of Short PEG on Near-Infrared BODIPY-Based Activatable Optical Probes. *ACS Omega* **2020**, *5*, 15657–15665.
- (7) Godard, A.; Kalot, G.; Pliquett, J.; Busser, B.; Le Guevel, X.; Wegner, K. D.; Resch-Genger, U.; Rousselin, Y.; Coll, J.-L.; Denat, F.; Bodio, E.; Goze, C.; Sancey, L. Water-Soluble Aza-BODIPYs: Biocompatible Organic Dyes for High Contrast In Vivo NIR-II Imaging. *Bioconjugate Chem.* **2020**, *31*, 1088–1092.
- (8) Schreiber, C. L.; Zhai, C.; Dempsey, J. M.; McGarraugh, H. H.; Matthews, B. P.; Christmann, C. R.; Smith, B. D. Paired Agent Fluorescence Imaging of Cancer in a Living Mouse Using Preassembled Squaraine Molecular Probes with Emission Wavelengths of 690 and 830 nm. *Bioconjugate Chem.* **2020**, *31*, 214–223.
- (9) Ogata, F.; Nagaya, T.; Maruoka, Y.; Akhigbe, J.; Meares, A.; Lucero, M. Y.; Satraitis, A.; Fujimura, D.; Okada, R.; Inagaki, F.; Choyke, P. L.; Ptaszek, M.; Kobayashi, H. Activatable Near-Infrared Fluorescence Imaging Using PEGylated Bacteriochlorin-Based Chlorin and BODIPY-Dyads as Probes for Detecting Cancer. *Bioconjugate Chem.* **2019**, *30*, 169–183.
- (10) Sun, Y.; Qu, C.; Chen, H.; He, M.; Tang, C.; Shou, K.; Hong, S.; Yang, M.; Jiang, Y.; Ding, B.; et al. Novel benzo-bis(1,2,5-thiadiazole) Fluorophores for In Vivo NIR-II Imaging of Cancer. *Chem. Sci.* **2016**, *7*, 6203–6207.

- (11) Lindsey, J.; et al. Near-infrared Tunable Bacteriochlorins Equipped for Bioorthogonal Labeling. *New J. Chem.* **2015**, *39*, 4534–4550.
- (12) Taniguchi, M.; Lindsey, J. S. Synthetic Chlorins, Possible Surrogates for Chlorophylls, Prepared by Derivatization of Porphyrins. *Chem. Rev.* **2017**, *117*, 344–535.
- (13) Yang, E.; Kirmaier, C.; Krayner, M.; Taniguchi, M.; Kim, H. J.; Diers, J. R.; Bocian, D. F.; Lindsey, J. S.; Holten, D. Photophysical Properties and Electronic Structure of Stable, Tunable Synthetic Bacteriochlorins: Extending the Features of Native Photosynthetic Pigments. *J. Phys. Chem. B* **2011**, *115*, 10801–10806.
- (14) Kee, H. L.; Kirmaier, C.; Tang, Q.; Diers, J. R.; Muthiah, C.; Taniguchi, M.; Laha, J. K.; Ptaszek, M.; Lindsey, J. S.; Bocian, D. F.; et al. Effects of Substituents on Synthetic Analogs of Chlorophylls. Part 2: Redox Properties, Optical Spectra and Electronic Structure. *Photochem. Photobiol.* **2007**, *83*, 1125–1143.
- (15) Kee, H. L.; Kirmaier, C.; Tang, Q.; Diers, J. R.; Muthiah, C.; Taniguchi, M.; Laha, J. K.; Ptaszek, M.; Lindsey, J. S.; Bocian, D. F.; et al. Effects of Substituents on Synthetic Analogs of Chlorophylls. Part 1: Synthesis, Vibrational Properties and Excited-state Decay Characteristics. *Photochem. Photobiol.* **2007**, *83*, 1110–1124.
- (16) Laha, J. K.; Muthiah, C.; Taniguchi, M.; Lindsey, J. S. A New Route for Installing the Isocyclic Ring on Chlorins Yielding 13 Δ 1-Oxophorbins. *J. Org. Chem.* **2006**, *71*, 7049–7052.
- (17) Yu, Z.; Pancholi, C.; Bhagavathy, G. V.; Kang, H. S.; Nguyen, J. K.; Ptaszek, M. Strongly Conjugated Hydroporphyrin Dyads: Extensive Modification of Hydroporphyrins' Properties by Expanding the Conjugated System. *J. Org. Chem.* **2014**, *79*, 7910–7925.
- (18) Lindsey, J.; et al. Bioconjugatable, Pegylated Hydroporphyrins for Photochemistry and Photomedicine. Narrow-Band, Red-Emitting Chlorins. *New J. Chem.* **2016**, *40*, 7721–7740.
- (19) Resch-Genger, U.; Grabolle, M.; Cavaliere-Jaricot, S.; Nitschke, R.; Nann, T. Quantum Dots Versus Organic Dyes as Fluorescent Labels. *Nat. Methods* **2008**, *5*, 763–775.
- (20) Murray, C. B.; Sun, S.; Gaschler, W.; Doyle, H.; Betley, T. A.; Kagan, C. R. Colloidal Synthesis of Nanocrystals and Nanocrystal Superlattices. *IBM J. Res. Dev.* **2001**, *45*, No. 47.
- (21) Williams, D. N.; Pramanik, S.; Brown, R. P.; Zhi, B.; McIntire, E.; Hudson-Smith, N. V.; Haynes, C. L.; Rosenzweig, Z. Adverse Interactions of Luminescent Semiconductor Quantum Dots with Liposomes and *Shewanella oneidensis*. *ACS Appl. Nano Mater.* **2018**, *1*, 4788–4800.
- (22) Hardman, R. A Toxicologic Review of Quantum Dots: Toxicity Depends on Physicochemical and Environmental Factors. *Environ. Health Perspect.* **2006**, *114*, 165.
- (23) Oh, E.; Rong, L.; Nel, A.; Gemill, K. B.; Bilal, M.; Yoram, C.; Medintz, I. L. Meta-analysis of cellular toxicity for cadmium-containing quantum dots. *Nat. Nanotechnol.* **2016**, *11*, 479–486.
- (24) Xu, G.; Lin, G.; Lin, S.; Wu, N.; Deng, Y.; Feng, G.; Chen, Q.; Qu, J.; Chen, D.; Chen, S.; Niu, H.; Mei, S.; Yong, K.-T.; Wang, X. The Reproductive Toxicity of CdSe/ZnS Quantum Dots on the In Vivo Ovarian Function and In Vitro Fertilization. *Sci. Rep.* **2016**, *6*, No. 37677.
- (25) Zhang, M.; Yue, J.; Cui, R.; Ma, Z.; Wan, H.; Wang, F.; Zhu, S.; Zhou, Y.; Kuang, Y.; Zhong, Y.; Pang, D.-W.; Dai, H. Bright Quantum Dots Emitting at Similar to 1,600 nm in the NIR-Iib Window for Deep Tissue Fluorescence Imaging. *Proc. Natl. Acad. Sci. U.S.A.* **2018**, *115*, 6590–6595.
- (26) Du, H.; Chialing, C.; Krishnan, R.; Krauss, T. D.; Harbold, J. M.; Wise, F. W.; Thomas, M. G.; Silcox, J. Optical Properties of Colloidal PbSe Nanocrystals. *Nano Lett.* **2002**, *2*, 1321–1324.
- (27) Tan, L.; Liu, S.; Li, X.; Chronakis, I. S.; Shen, Y. A New Strategy for Synthesizing AgInS₂ Quantum Dots Emitting Brightly in Near-Infrared Window for In Vivo Imaging. *Colloids Surf., B* **2015**, *125*, 222–229.
- (28) Che, D.; Di, D.; Hongzhi, W.; Qinghong, Z.; Yaogang, L. Aqueous Synthesis of High Bright Ag₂SeZnSe Quantum Dots with Tunable Near-Infrared Emission. *J. Alloys Compd.* **2016**, *678*, 51–56.
- (29) Gil, H. M.; Price, T. W.; Chelani, K.; Bouillard, J.-S. G.; Calaminus, S. D. J.; Stasiuk, G. J. NIR-Quantum Dots in Biomedical Imaging and their Future. *iScience* **2021**, *24*, No. 102189.
- (30) Li, J.; Jianghong, R.; Kanyi, P. Recent Progress on Semiconducting Polymer Nanoparticles for Molecular Imaging and Cancer Phototherapy. *Biomaterials* **2018**, *155*, 217–235.
- (31) Pecher, J.; Mecking, S. Nanoparticles of Conjugated Polymers. *Chem. Rev.* **2010**, *110*, 6260–6279.
- (32) Wu, C.; Schneider, T.; Zeigler, M.; Yu, J.; Schiro, P. G.; Burnham, D. R.; McNeill, J. D.; Chiu, D. T. Bioconjugation of Ultrabright Semiconducting Polymer Dots for Specific Cellular Targeting. *J. Am. Chem. Soc.* **2010**, *132*, 15410–15417.
- (33) Wu, C.; Bull, B.; Szymanski, C.; Christensen, K.; McNeill, J. Multicolor Conjugated Polymer Dots for Biological Fluorescence Imaging. *ACS Nano* **2008**, *2*, 2415–2423.
- (34) Xu, T.; Yu, L. How to Design Low Bandgap Polymers for Highly Efficient Organic Solar Cells. *Mater. Today* **2014**, *17*, 11–15.
- (35) Rohatgi, C. V.; Harada, T.; Need, E. F.; Krasowska, M.; Beattie, D. A.; Dickenson, G. D.; Smith, T. A.; Kee, T. W. Low-Bandgap Conjugated Polymer Dots for Near-Infrared Fluorescence Imaging. *ACS Appl. Nano Mater.* **2018**, *1*, 4801–4808.
- (36) Ke, C.-S.; Fang, C.-C.; Yan, J.-Y.; Tseng, P.-J.; Pyle, J. R.; Chen, C.-P.; Lin, S.-Y.; Chen, J.; Zhang, X.; Chan, Y.-H. Molecular Engineering and Design of Semiconducting Polymer Dots with Narrow-Band, Near-Infrared Emission for in Vivo Biological Imaging. *ACS Nano* **2017**, *11*, 3166–3177.
- (37) Chen, L.; Chen, D.; Jiang, Y.; Zhang, J.; Yu, J.; DuFort, C. C.; Hingorani, S. R.; Zhang, X.; Wu, C.; Chiu, D. T. A BODIPY-Based Donor/Donor–Acceptor System: Towards Highly Efficient Long-Wavelength-Excitable Near-IR Polymer Dots with Narrow and Strong Absorption Features. *Angew. Chem., Int. Ed.* **2019**, *58*, 7008–7012.
- (38) Jin, Y.; Ye, F.; Zeigler, M.; Wu, C.; Chiu, D. T. Near-Infrared Fluorescent Dye-Doped Semiconducting Polymer Dots. *ACS Nano* **2011**, *5*, 1468–1475.
- (39) Chen, D.; Wu, L. C.; Liu, Z.; Tang, Y.; Chen, H.; Yu, J.; Wu, C.; Chiu, D. T. Semiconducting Polymer Dots with Bright Narrow-Band Emission at 800 nm for Biological Applications. *Chem. Sci.* **2017**, *8*, 3390.
- (40) Chen, S.; Cui, S.; Du, R.; Liu, M.; Tsai, W.-K.; Guo, F.; Wu, Q.; Zhao, L.; Zhang, Y. Simultaneous Near-Infrared and Green Fluorescence from Single Conjugated Polymer Dots with Aggregation-Induced Emission Fluorogen for Cell Imaging. *J. Mater. Chem. B* **2018**, *6*, 7871–7876.
- (41) Gupta, N.; Chan, Y. H.; Saha, S.; Liu, M. H. *Near-Infrared-II Semiconducting Polymer Dots for Deep-Tissue Fluorescence Imaging*, Wiley, 2021; Vol. 16, pp 175–184.
- (42) Paisley, N. R.; Halldorson, S. V.; Tran, M. V.; Gupta, R.; Kamal, S.; Algar, W. R.; Hudson, Z. M. Near-Infrared-Emitting Boron-Difluoride-Curcuminoid-Based Polymers Exhibiting Thermally Activated Delayed Fluorescence as Biological Imaging Probes. *Angew. Chem., Int. Ed.* **2021**, *60*, 18630–18638.
- (43) Rauch, M. F.; Michaud, M.; Hao, X.; Madri, J. A.; Lavik, E. B. Co-culture of Primary Neural Progenitor and Endothelial Cells in a Macroporous Gel Promotes Stable Vascular Networks In Vivo. *J. Biomater. Sci., Polym. Ed.* **2008**, *19*, 1469–1485.
- (44) Meares, A.; Bhagavathy, G. V.; Zik, S. R.; Gallagher, T.; Ptaszek, M. Expanding pi-Conjugation in Chlorins Using Ethenyl Linker. *J. Org. Chem.* **2018**, *83*, 9076–9087.
- (45) Muthiah, C.; Lahaye, D.; Taniguchi, M.; Ptaszek, M.; Lindsey, J. S. Regioselective Bromination Tactics in the de Novo Synthesis of Chlorophyll b Analogues. *J. Org. Chem.* **2009**, *74*, 3237–3247.
- (46) Muthiah, C.; Ptaszek, M.; Nguyen, T. M.; Flack, K. M.; Lindsey, J. S. Two Complementary Routes to 7-Substituted Chlorins. Partial Mimics of Chlorophyll b. *J. Org. Chem.* **2007**, *72*, 7736–7749.
- (47) Krayner, M.; Ptaszek, M.; Kim, H. J.; Meneely, K. R.; Fan, D.; Secor, K.; Lindsey, J. S. Expanded Scope of Synthetic Bacteriochlorins via Improved Acid Catalysis Conditions and Diverse Dihydropyrrin-Acetals. *J. Org. Chem.* **2010**, *75*, 1016–1039.

(48) Wang, D.; Liu, J.; Liu, Z.; Zhang, Z.; Sun, Z.; Wu, C.; Wang, G. Bioconjugation of IgG Secondary Antibodies to Polymer Dots for Multicolor Subcellular Imaging. *ACS Appl. Nano Mater.* **2020**, *3*, 2214–2220.

(49) Clough, S. J.; Bent, A. F. *Floral Dip: A Simplified Method for Agrobacterium-Mediated Transformation of Arabidopsis thaliana*, BIOS Scientific Publishers & Blackwell Scientific Publications: Great Britain, 1998; Vol. 16, pp 735–743.

(50) Taniguchi, M.; Cramer, D.; Bhise, A.; Kee, H.; Bocian, D.; Holten, D.; Lindsey, J. Accessing the Near-Infrared Spectral Region with Stable, Synthetic, Wavelength-Tunable Bacteriochlorins. *New J. Chem.* **2008**, *32*, 947–958.

(51) Yang, E.; Ruzi, C.; Krayner, M.; Diers, J. R.; Niedzwiedzki, D. M.; Kirmaier, C.; Lindsey, J. S.; Bocian, D. F.; Holten, D. Photophysical Properties and Electronic Structure of Bacteriochlorin-Chalcones with Extended Near-Infrared Absorption. *Photochem. Photobiol.* **2013**, *89*, 586–604.

(52) Frank, P. G.; Woodman, S. E.; Park, D. S.; Lisanti, M. P. Caveolin, Caveolae, and Endothelial Cell Function. *Arteriosclerosis Thromb. Vasc. Biol.* **2003**, *23*, 1161–1168.

(53) Li, H.-H.; Li, J.; Wasserloos, K. J.; Wallace, C.; Sullivan, M. G.; Bauer, P. M.; Stolz, D. B.; Lee, J. S.; Watkins, S. C.; St Croix, C. M.; Pitt, B. R.; Zhang, L.-M. Caveolae-Dependent and -Independent Uptake of Albumin in Cultured Rodent Pulmonary Endothelial Cells. *PLoS One* **2013**, *8*, No. e81903.

(54) Wyrsh, I.; Ana, D.-F.; Niko, G.; Thomas, B. Tissue-specific FLAGELLIN-SENSING 2 (FLS2) Expression in Roots Restores Immune Responses in Arabidopsis fls2 Mutants. *New Phytol.* **2015**, *206*, 774–784.

(55) Bücherl, C. A.; Jarsch, I. K.; Schudoma, C.; Segonzac, C.; Mbengue, M.; Robatzek, S.; MacLean, D.; Ott, T.; Zipfel, C. Plant Immune and Growth Receptors Share Common Signalling Components but Localise to Distinct Plasma Membrane Nano-domains. *eLife* **2017**, *6*, No. e25114.

(56) Rust, M. J.; Bates, M.; Xiaowei, Z. Sub-Diffraction-Limit Imaging by Stochastic Optical Reconstruction Microscopy (STORM). *Nat. Methods* **2006**, *3*, 793–796.

(57) Betzig, E.; George, H. P.; Rachid, S.; Lindwasser, O. W.; Scott, O.; Juan, S. B.; Michael, W. D.; Jennifer, L.-S.; Harald, F. H. Imaging Intracellular Fluorescent Proteins at Nanometer Resolution. *Science* **2006**, *313*, 1642.

NOTE ADDED AFTER ASAP PUBLICATION

This paper was published ASAP on April 22, 2022, with an incorrect Supporting Information file due to a production error. The corrected version was reposted on April 25, 2022.

Recommended by ACS

An Effective Supramolecular Approach to Boost the Photodynamic Therapy Efficacy of a Near-Infrared Activating Perylene Diimide-Based Photosensitizer

Chengwei Li, Jian Zhao, *et al.*

MARCH 09, 2022
ACS MATERIALS LETTERS

READ 

High Singlet Oxygen Yield Photosensitizer Based Polypeptide Nanoparticles for Low-Power Near-Infrared Light Imaging-Guided Photodynamic Therapy

Zheng Ruan, Lifeng Yan, *et al.*

SEPTEMBER 06, 2018
BIOCONJUGATE CHEMISTRY

READ 

Bioconjugation of IgG Secondary Antibodies to Polymer Dots for Multicolor Subcellular Imaging

Dan Wang, Guofeng Wang, *et al.*

JANUARY 16, 2020
ACS APPLIED NANO MATERIALS

READ 

AIE-Active Fluorescent Nonconjugated Polymer Dots for Dual-Alternating-Color Live Cell Imaging

Xiaolin Guan, Ziqiang Lei, *et al.*

OCTOBER 15, 2018
INDUSTRIAL & ENGINEERING CHEMISTRY RESEARCH

READ 

Get More Suggestions >